Importance of crustal corrections in the development of a new global model of radial anisotropy

M. P. Panning,[1] V. Lekić,[2,3] and B. A. Romanowicz[2]

Received 2 March 2010; revised 31 August 2010; accepted 20 September 2010; published 24 December 2010.

[1] Accurately inferring the radially anisotropic structure of the mantle using seismic waveforms requires correcting for the effects of crustal structure on waveforms. Recent studies have quantified the importance of accurate crustal corrections when mapping upper mantle structure using surface waves and overtones. Here, we explore the effects of crustal corrections on the retrieval of deep mantle velocity and radial anisotropy structure. We apply a new method of nonlinear crustal corrections to a three-component surface and body waveform data set and invert for a suite of models of radially anisotropic shear velocity. We then compare the retrieved models against each other and a model derived from an identical data set but using a different nonlinear crustal correction scheme. While retrieval of isotropic structure in the deep mantle appears to be robust with respect to changes in crustal corrections, we find large differences in anisotropic structure that result from the use of different crustal corrections, particularly at transition zone and greater depths. Furthermore, anisotropic structure in the lower mantle, including the depth-averaged signature in the core-mantle boundary region, appears to be quite sensitive to choices of crustal correction. Our new preferred model, SAW642ANb, shows improvement in data fit and reduction in apparent crustal artifacts. We argue that the accuracy of crustal corrections may currently be a limiting factor for improved resolution and agreement between models of mantle anisotropy.

Citation: Panning, M. P., V. Lekić, and B. A. Romanowicz (2010), Importance of crustal corrections in the development of a new global model of radial anisotropy, *J. Geophys. Res.*, *115*, B12325, doi:10.1029/2010JB007520.

1. Introduction

[2] Global seismic tomography shows excellent promise for illuminating current mantle flow patterns. In particular, isotropic models have shown strong convergence in the long-wavelength structure, and have been revealing finer and finer details in structure of isotropic S velocity [*Mégnin and Romanowicz*, 2000; *Gu et al.*, 2003; *Ritsema et al.*, 2004; *Montelli et al.*, 2006; *Houser et al.*, 2008; *Simmons et al.*, 2009] as well as P velocity [*Montelli et al.*, 2004; *Li et al.*, 2006; *Houser et al.*, 2008]. These provide an excellent constraint on the current mantle thermal structure under the assumption that lateral velocity perturbations can be explained primarily as thermal variations. Using this assumption, the models can then be related to mantle flow by determining the associated density perturbations due to the thermal structure. Some models [e.g., *Simmons et al.*, 2009] attempt to incorporate other geodynamic data such as free-air gravity data and dynamic topography to more directly constrain the density field driving flow, but, in general, isotropic models allow for only an indirect connection with mantle flow patterns.

[3] Models including anisotropic structure, however, have the potential to more directly illuminate flow. This is because dynamic processes in the mantle can produce seismically observable anisotropy either through alignment of contrasting materials and melt (shape preferred orientation or SPO) or the alignment of the crystallographic axes of intrinsically anisotropic minerals (lattice preferred orientation or LPO). Kinematic modeling of LPO [*Kaminski and Ribe*, 2001] produced through mantle flow models [e.g., *Becker et al.*, 2008] suggest that upper mantle anisotropy can be well modeled using such an approach, but care must be taken in interpreting the results as different LPO deformation modes are possible [*Karato et al.*, 2008].

[4] At this time, several global models of radial anisotropy, where a vertical axis of symmetry is assumed, are available [*Boschi and Dziewonski*, 2000; *Beghein and Trampert*, 2004a; *Panning and Romanowicz*, 2006; *Kustowski et al.*, 2008], but as pointed out by *Becker et al.* [2008], significant differences remain between anisotropic models. In order to provide robust constraints on geodynamic modeling, it is clear that there needs to be some convergence between different models to increase confidence in the resolved structures.

[5] One potential source of errors and inconsistencies between anisotropic models is through the use of crustal corrections, which attempt to remove the signals that arise

[1]Department of Geological Sciences, University of Florida, Gainesville, Florida, USA.
[2]Berkeley Seismological Laboratory, University of California, Berkeley, California, USA.
[3]Now at Department of Geological Sciences, Brown University, Providence, Rhode Island, USA.

0148-0227/10/2010JB007520

due to crustal structure from those originating in the mantle. As pointed out by *Bozdağ and Trampert* [2008], crustal corrections have a different impact on Love and Rayleigh waves, and thus imperfect crustal corrections have the potential to bias models of radial anisotropy in the upper mantle. These findings were confirmed by *Lekić et al.* [2010], who extended this analysis to the full waveforms of both surface waves and overtones. However, no quantitative analysis has yet been performed to investigate the effect of imperfect crustal corrections on a complete long-period waveform data set including both body and surface waves, and the associated potential contamination of deep mantle structure. This is one of the goals of our study.

[6] Accurate crustal corrections are, however, nontrivial to perform. One computationally inexpensive approach is to model the crustal effects as linear perturbations in topography of the surface/seafloor and Mohorovičić discontinuity (or Moho) from a reference model, and this approach has been used in the development of many tomographic models, including an earlier model developed from the same data set applied here [*Panning and Romanowicz*, 2004]. However, the crust clearly has very strong heterogeneity in both thickness and velocity structure and strongly deviates from linearity. *Boschi and Ekström* [2002] attempted to account for this nonlinearity by calculating surface wave modes for the appropriate crustal structure at each point along the path between source and receiver. Another approach to dealing with this nonlinearity, proposed by *Montagner and Jobert* [1988], is to divide the Earth into a set of tectonic regions. Within each region, a different reference model is defined which can be used to calculate appropriate eigenfunctions for surface waves or normal modes. These different regionalized models can include crustal thicknesses and velocity structures different from the global reference model. This would then capture most of the nonlinearity due to strong deviations from a single global reference model, while further deviations could then be modeled linearly. This approach has the additional benefit of allowing sensitivity to deeper velocity structure to also be calculated using the suite of tectonic models, therefore capturing nonlinearity introduced in that fashion as well. This approach was independently refined by *Marone and Romanowicz* [2007] and *Kustowski et al.* [2007], and implemented in the creation of two recent anisotropic models [*Panning and Romanowicz*, 2006; *Kustowski et al.*, 2008]. However, as pointed out earlier, there are still many differences between the anisotropic structure in these two models. Is there another way to better model crustal effects? Recently, *Lekić et al.* [2010] have proposed a more computationally inexpensive way of capturing the nonlinear effects of crustal structure. This method, like that proposed by *Montagner and Jobert* [1988], relies on first defining a suite of tectonic regions. However, rather than using these models to define a new set of eigenfunctions, in this method we simply invert for the appropriate perturbations to the crustal model that account for the nonlinearity for different subsets of modes (e.g., fundamental mode Love and Rayleigh waves and overtones). When performing the actual inversion, we only need to use the appropriate modified crustal model rather than tracking multiple crustal models and sets of eigenfunctions. At first glance, it might appear that this simplified approach may not capture the nonlinearity as well as the *Montagner and Jobert* [1988] approach, but numerical simulations suggest the method performs quite well [*Lekić et al.*, 2010].

[7] In this study, we quantify the contamination of deep mantle velocity and anisotropic structure that can result from different ways of performing crustal corrections. Our work complements the analyses carried out previously by *Bozdağ and Trampert* [2008] and *Lekić et al.* [2010] on surface waves and overtones, respectively. We do this by applying different implementations of the computationally efficient "modified linear corrections" (MLC) approach of *Lekić et al.* [2010] to develop a suite of global radially anisotropic models using the same parameterization and data set as that used in the development of the global model SAW642AN [*Panning and Romanowicz*, 2006]. By contrasting the retrieved velocity and anisotropic structures between these models and SAW642AN, which was developed using a different nonlinear crustal corrections technique based on the *Marone and Romanowicz* [2007] approach (hereafter referred to as NLC), we will demonstrate that crustal corrections can substantially affect the retrieval of anisotropic structure in the deep mantle, even in the D″ region. Finally, we will present a preferred radially anisotropic mantle model, SAW642ANb, constructed using MLC and capable of providing a better overall fit to the data even with smaller overall model size, while removing some signatures in the isotropic portion of SAW642AN that appear to be crustal artifacts.

2. Modeling Approach

[8] The models presented here are developed with the same parameterization and waveform data set as used in the development of SAW642AN [*Panning and Romanowicz*, 2006]. Additionally, the same basic theory, nonlinear asymptotic coupling theory (NACT) [*Li and Romanowicz*, 1995], is used to model the waveforms as in that model. We will briefly describe this theory and the waveform data set here, but more detailed explanations are given by *Panning and Romanowicz* [2006] and *Li and Romanowicz* [1995].

2.1. Waveform Data Set and Theory

[9] The waveform data used in this study consist of three-component broadband surface waveforms (short-period corner of 80 s and cutoff of 60 s) as well as body waveforms (short period corner of 40 s and cutoff of 32 s). The waveforms are windowed to separate various energy wave packets (e.g., separating fundamental mode and overtone surface waves, as well as different body wave energy packets), which enhances resolution of transition zone and lower mantle structure [*Mégnin and Romanowicz*, 1999]. The final data set includes over 120,000 wave packets with over 4 million data points (Table 1) [*Panning and Romanowicz*, 2006].

[10] The waveforms and their sensitivity to anisotropic velocity structure are modeled using NACT [*Li and Romanowicz*, 1995]. This theory is a normal mode based perturbation approach that includes both along branch and cross-branch coupling of modes in order to develop 2-D sensitivity kernels in the vertical plane defined by the great circle path between source and receiver. This theory brings out the ray character of sensitivity while also including some of the off-path sensitivity due to finite frequency effects. It also includes effects of multiple forward scattering [*Romanowicz et al.*, 2008; *Panning et al.*, 2009].

Table 1. Percent Variance Reduction for Data Subsets[a]

Data Set	SAW642AN	Model A	Model B	Model C	Model D
Fundamental	60.8	61.8	61.9	62.0	61.7
Overtones	48.7	51.8	52.1	52.7	52.1
Total surface wave	56.2	57.9	58.1	58.4	58.0
Body waves	44.8	46.5	47.9	49.1	45.4
Total	52.1	53.8	54.5	55.1	53.5

[a]Note that all variance reduction numbers are calculated with the crustal corrections used in their development (NLC for SAW642AN, MLC for models A–C, MLC for model D surface waves, and NLC for model D body waves).

[11] As in SAW642AN, the model is parameterized in terms of the Voigt average isotropic S velocity, V_S, and the anisotropic parameter ξ, which can be written in terms of the horizontally and vertically polarized S velocities (V_{SH} and V_{SV}, respectively) as

$$V_S^2 = \frac{2V_{SV}^2 + V_{SH}^2}{3} \tag{1}$$

$$\xi = \frac{V_{SH}^2}{V_{SV}^2}. \tag{2}$$

We also assume the same scaling relationships for perturbations to P velocity and the other two anisotropic parameters as in the development of SAW642AN. While many mathematically equivalent parameterizations are possible, we choose this one rather than one with separate V_{SH} and V_{SV} models, for example, because it allows us to tune damping specifically on the anisotropic portion of the model. With separate inversions, where the anisotropy is proportional to the difference between the two models, the uncertainty becomes quite large, and it is difficult to constrain the anisotropy to be small in order to test whether anisotropy is really required by the data.

[12] Finally, the spatial parameterization of the model is the same as SAW642AN, with 16 variably spaced cubic b splines with depth [*Mégnin and Romanowicz*, 2000], and 642 equally spaced spherical splines laterally [*Wang and Dahlen*, 1995]. This provides a nominal lateral resolution of ~800 km, and variable depth resolution that is approximately scaled with data coverage.

2.2. Improved Crustal Corrections

[13] The first anisotropic model developed with this data set [*Panning and Romanowicz*, 2004, hereafter referred to as PR04] was developed with simple linear crustal corrections, although separate crustal models were used for the portions of the data primarily sensitive to V_{SH} or V_{SV}. In classical normal mode theory, the linear effect of crustal structure can be written

$$\delta\omega_k^2 = 2\omega_k\delta\omega_k = \sum_d r_d^2 h_d(\theta,\phi) H_k^d(\theta,\phi), \tag{3}$$

where $\delta\omega_k$ is the eigenfrequency perturbation of the kth normal mode, r_d is the radius of the dth discontinuity in the global reference model, h_d represents the perturbations in topography, and H_d is the calculated sensitivity to discontinuity topography.

[14] In the development of SAW642AN, we attempted to improve the crustal corrections by implementing the hereafter MR07 *Marone and Romanowicz* [2007] nonlinear crustal corrections, an approach we will henceforth refer to as NLC. In this approach, we defined a suite of models for 5 tectonic regions based on CRUST2.0 [*Bassin et al.*, 2000], and calculated the appropriate eigenfunctions for each model. Each of these models differed from the global reference model in both thickness and velocity structure, with the regionalized models having a three-layer velocity structure simplified from CRUST2.0. At each point along the path between source and receiver we then calculated a crustal correction term that had a nonlinear portion due to the difference in eigenfrequency between the tectonic model and PREM, as well as further linear corrections for the deviation from the regionalized model. Additionally, we used sensitivity kernels calculated from the appropriate regionalized eigenfunctions. We can summarize this approach as treating the perturbation of a mode k from a global reference model (GRM) as the sum of a linear perturbation from a local reference model (LRM) plus the difference between the eigenfrequency of the mode in the GRM and the LRM, e.g.,

$$2\omega_k\delta\omega_k = \sum_d \left(r_d^{LRM}\right)^2 h_d^{LRM}(\theta,\phi) H_k^{d,LRM}(\theta,\phi) + \omega_k^{LRM} - \omega_k^{(GRM)}, \tag{4}$$

where ω_k^{LRM} and ω_k^{GRM} are the eigenfrequencies in the local and global reference models, respectively, and the sensitivity is now explicitly calculated in the local reference model (see equations (1) and (2) of MR07).

[15] The NLC approach is fairly computationally intensive, primarily due to the input/output requirements necessary to track eigenfunctions and kernels for multiple models. In order to ideally obtain a similar level of approximation to the nonlinear problem of crustal corrections with a less computationally intensive approach, *Lekić et al.* [2010] have recently proposed an alternative approach of modified linear corrections (MLC). We start by rewriting the standard way of expressing linear crustal corrections due to topography of the surface and Moho (equation (3)) in a matrix form as

$$\mathbf{w} = \mathbf{H}\delta\mathbf{r}, \tag{5}$$

where $\mathbf{w}$ is a column vector of length N (the number of modes considered) with the kth element defined by $2\omega_k\delta\omega_k$, the eigenfrequency perturbation to the kth mode, $\mathbf{H}$ is a $2 \times N$ matrix summarizing the sensitivity to topography of the two boundaries (e.g., elements can be written as $r_d^2 H_k^d$), and $\delta\mathbf{r}$ is the perturbation of the two boundaries. In the NLC approach, we divide $\mathbf{w}$ into two terms (a nonlinear and a linear one), where the linear one is defined by making the appropriate changes to $\mathbf{H}$ for the different tectonic models. In the new MLC approach, we choose to instead represent the nonlinearity by adding in a term to the topography perturbations, writing instead

$$\mathbf{w} = \mathbf{H}(\delta\mathbf{r} + \mathbf{c}_{md}), \tag{6}$$

where the subscripts m and d indicate that we invert for different correction factors for different mode types m (separating out spheroidal and toroidal modes, as well as

fundamental and overtone modes), and different discontinuities d (Moho and surface topography). The inversion is done to minimize the difference between eigenfrequencies calculated with this correction compared to those calculated directly from each tectonic model (which once again includes differences from the global model in both crustal thickness and velocity structure). Unlike the NLC approach, once the correction factors are precalculated, there is no additional computational cost when inverting as compared to linear corrections, which makes using larger numbers of crustal models more practical. In this study, we utilize 7 different tectonic regions [as defined by *Lekić et al.* [2010] based on CRUST2.0 and only consider corrections to the Moho topography. Even larger numbers of regions could be utilized to more accurately reflect the crust with only a relatively small increase in time necessary to precompute the correction factors, but no increase in the computational costs of the actual inversion. As a drawback, however, we lose the ability in this method to define kernels using eigenfunctions in the regionalized models. Additionally, there is an implicit assumption that only self-coupling is important, which may be adequate for fundamental modes (although coupling between fundamental Love and Rayleigh modes has been shown to be important in the presence of anisotropy [e.g., *Park*, 1993; *Beghein et al.*, 2008]), but is even more problematic for surface wave overtones, and generally not adequate to describe body wave sensitivity. While there are therefore some trade-offs between the methods in terms of the modeling of the nonlinearity, *Lekić et al.* [2010] showed significant improvement over standard linear corrections, based on numerical testing.

3. Results

[16] We applied this new MLC approach to crustal corrections and performed 4 additional model inversion iterations starting from SAW642AN. Three classes of models were created, based upon the corrections used for the body wave portion of the data set. As discussed in section 2.2, these crustal corrections are derived separately for fundamental and overtone surface waves. However, no explicit correction for body waves is developed, as the method implicitly only includes self-coupling, which is not correct for body wave sensitivity. With that in mind, we attempted to do the inversion with three different approaches for the body wave corrections: (1) linear corrections only from CRUST2.0, (2) the corrections derived for the overtone modes, or (3) the NLC corrections used in the development of SAW642AN. For the rest of the paper, we will be referring to four models (A, B, C, and D). Model A includes only the linear corrections for body wave packets (while still utilizing MLC corrections for the fundamental mode and overtone surface waves), while B and C use the overtone-derived corrections for the body waves. Model D was derived using the NLC corrections for the body wave data. Damping for all 4 models was chosen in order to produce a similar model size for the isotropic portion of the model as in SAW642AN, as defined by the root mean squared amplitude as a function of depth (Figure 1). The damping for the anisotropic portion of models A and B was chosen so as to strongly reduce the amplitude of anisotropy at transition zone and greater depths (Figure 2), for reasons to be discussed later, while models C and D have similar anisotropic amplitudes to SAW642AN.

[17] The variance reduction numbers for models A, B, C, and D as discussed above, as well as SAW642AN are summarized in Table 1. All four models are able to achieve superior variance reduction as compared to SAW642AN with the NLC crustal corrections for the entire data set. Model B is able to achieve slightly better fit than model A with similar model size, which suggests that applying the overtone based correction to the body waves provides an improvement over simple linear corrections. Model C shows slightly better data fit, although with a more strongly anisotropic model, which means there were more effective model parameters. Despite a similar model size to model C, model D has the worse data fit of the four new models, suggesting that in this case, the NLC corrections for the body wave data do not show improvement relative to the MLC corrections. However, all of the changes in fit between the models discussed here are small and dependent on the damping choices made in the inversion, and so it is difficult to make a statistical argument for one model over another. A simple application of the F test with degrees of freedom defined as $n-p$, where n is the number of wave packets in the inversion and p the number of model parameters, would suggest that an estimated variance ratio as small as 1.01 (corresponding to an overall variance reduction of >52.7%) would be significantly improved fit over SAW642AN at the 95% confidence level, meaning that all four models have statistically significant improved fit relative to SAW642AN. However, such a test is questionable in this situation where assumptions of data independence are likely violated, and so this can only be treated as a lower bound of the real confidence threshold. For example, reducing the number of degrees of freedom by a factor of 10 (as an estimated upper bound) increases the required variance reduction threshold for 95% confidence to 55.8%, which would mean that models A–D are just short of a statistically significant improvement in fit over SAW642AN. Regardless, it is clear that the differences between each of these models as well as relative to SAW642AN are small, but quite close to a 95% confidence threshold.

3.1. Isotropic V_S Structure

[18] The isotropic V_S structure is quite similar to SAW642AN, as well as other global shear velocity models (shown for model B in Figure 3). As usual we see tectonic structure at shallow depths with strong difference in oceanic and continental velocities, and a general trend of increasing velocity as a function of age in the oceanic regions. As we move down into the transition zone, the strongest anomalies are associated with regions of subduction, while the amplitude of structure becomes much smaller through midmantle depth ranges. Finally, we see a degree 2 pattern in the core-mantle boundary region, with a fast ring around the two large low-velocity provinces often called the superplumes.

[19] In order to quantify differences between models, we also calculated the correlation of the isotropic portions of models A, B, C, and D to SAW642AN as a function of depth (Figure 4). These correlations are calculated by expanding the models in spherical harmonics to degree 24 at each depth, and then calculating the correlation across those spherical harmonic coefficients. This approach also allows us to define an

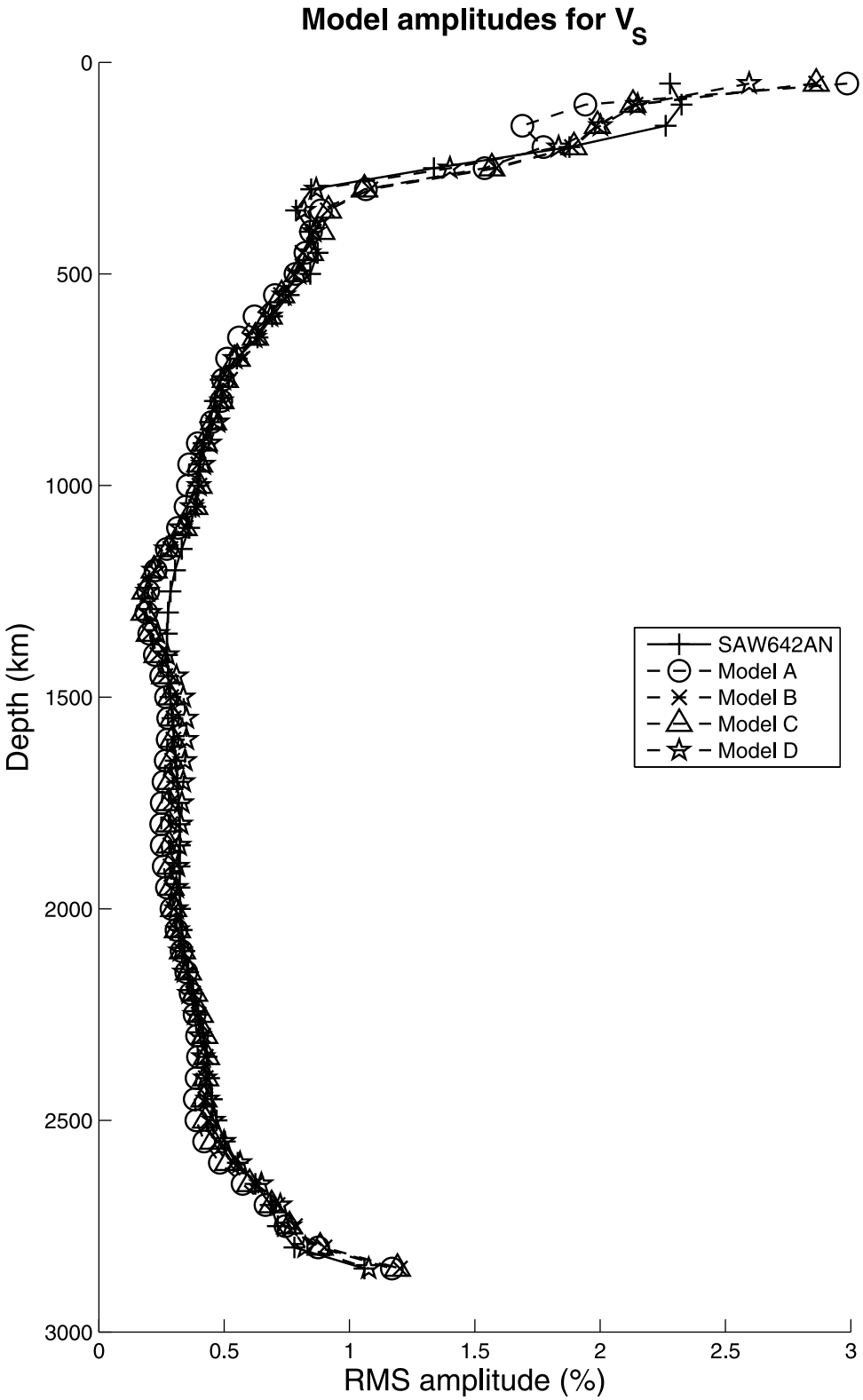

Figure 1. Root-mean-square amplitude (in percent perturbation) for the isotropic V_S portion of SAW642AN (black solid line), as well as models A, B, C, and D as discussed in the text (with symbols defined in legend).

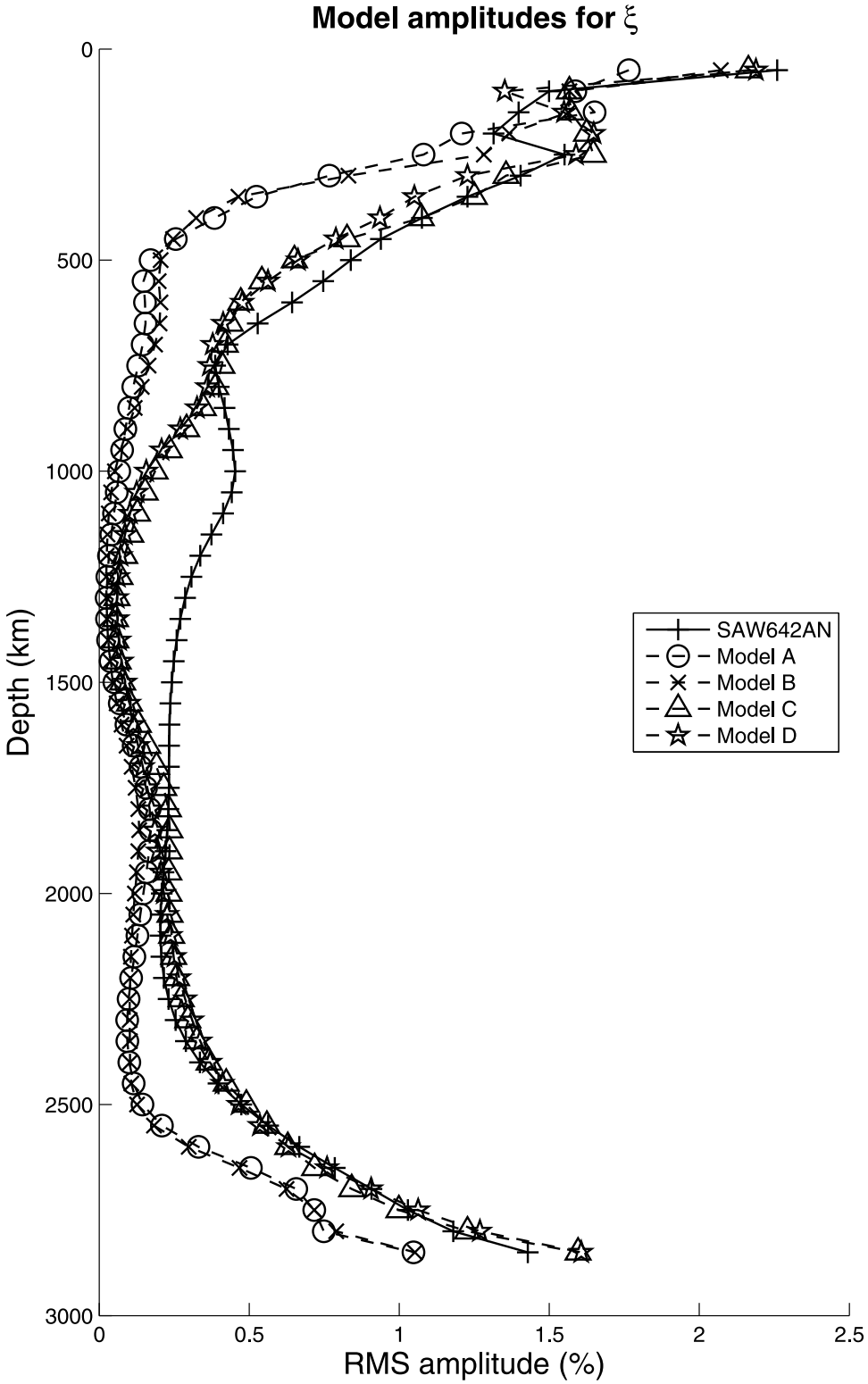

Figure 2. Same as Figure 1 but for perturbations in ξ.

effective number of model parameters at each depth, by determining the angular order l_{max} necessary to explain 98% of the power of the model at that depth, and then defining the effective number of model parameters at each depth by the number of spherical harmonic coefficients needed, $n_{eff} = (l_{max} + 1)^2$. Given that number of effective model parameters, we can then also define a 95% significance threshold for the correlation coefficient relative to the null hypothesis of decorrelated models. Unsurprisingly, the correlation for all three models greatly exceeds the 95% significance threshold,

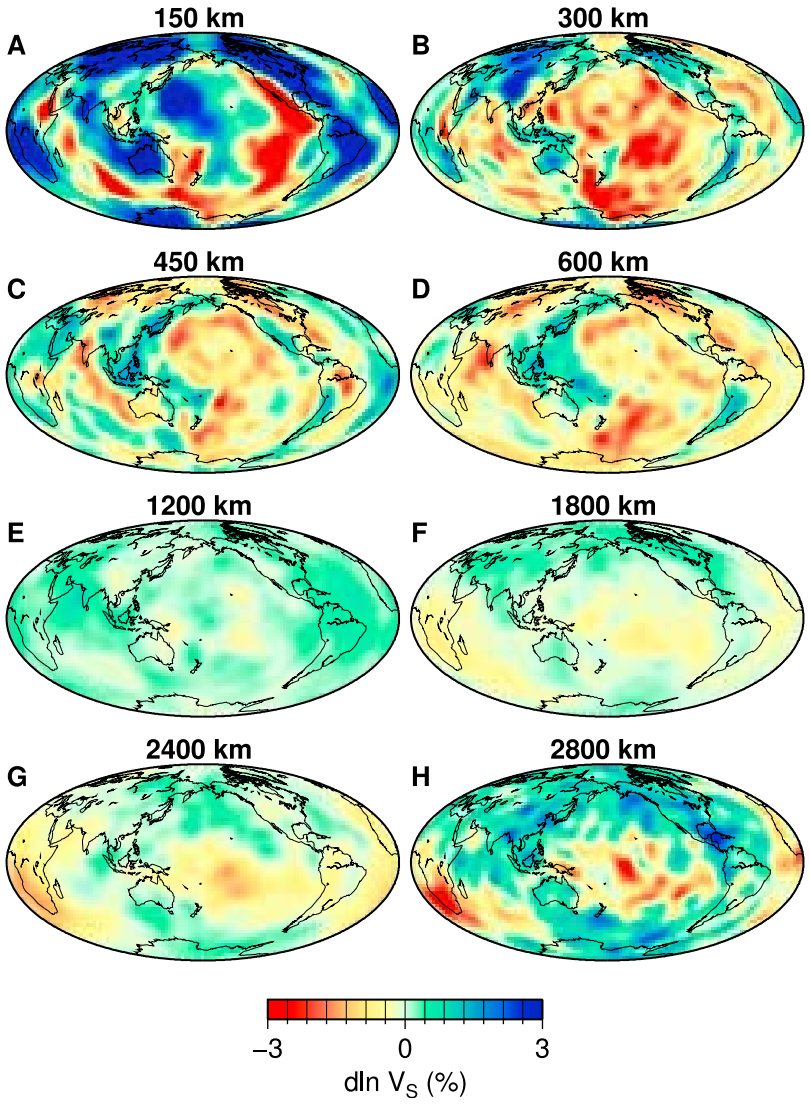

Figure 3. Perturbations in V_S plotted for several depths in the mantle for model B discussed in the text. All slices use the same color scale defined in color bar. Values are perturbations in percent from the velocity of the reference model PREM.

although there are larger changes in structure in the transition zone and the upper portion of the lower mantle (~400–1500 km) as compared to the uppermost and lowermost mantle. Since the structure at these depth ranges where we are seeing differences is primarily controlled by the body wave data, it is unsurprising that model D, which uses the same crustal corrections for body waves as in the development of SAW642AN, remains highly correlated in all depth ranges. It should be noted here that the F test used to determine the 95% confidence level assumes independent realizations of the models, while models A–D are all the products of damped nonlinear inversions starting from SAW642AN, which would indicate that the models are not entirely independent from SAW642AN and therefore should require a larger correlation coefficient for 95% confidence. However, 4 iterations were performed from the starting model, with damping at each step penalizing large values relative to the reference model PREM rather than the starting model, and therefore the assumption of independence should be reasonable.

[20] While the changes in these transition zone and midmantle depth ranges are not particularly apparent when comparing maps on global scales, such as in Figure 3, the differences become more clear when comparing the radial correlation functions of the different models (Figure 5). Radial correlation functions plot the correlation coefficient between different depths of the same model. In SAW642AN, there is a fairly strong anticorrelation between the shallow tectonically dominated structure and the structure of the transition zone and the uppermost lower mantle between 600 and 1000 km. Additionally, we see a strong positive correlation develop between the uppermost mantle and the midmantle depths between 1000 and 2000 km depth. While it is possible that such structure could reflect the real velocity structure of the Earth, it is not generally present in other global models of shear velocity structure such as

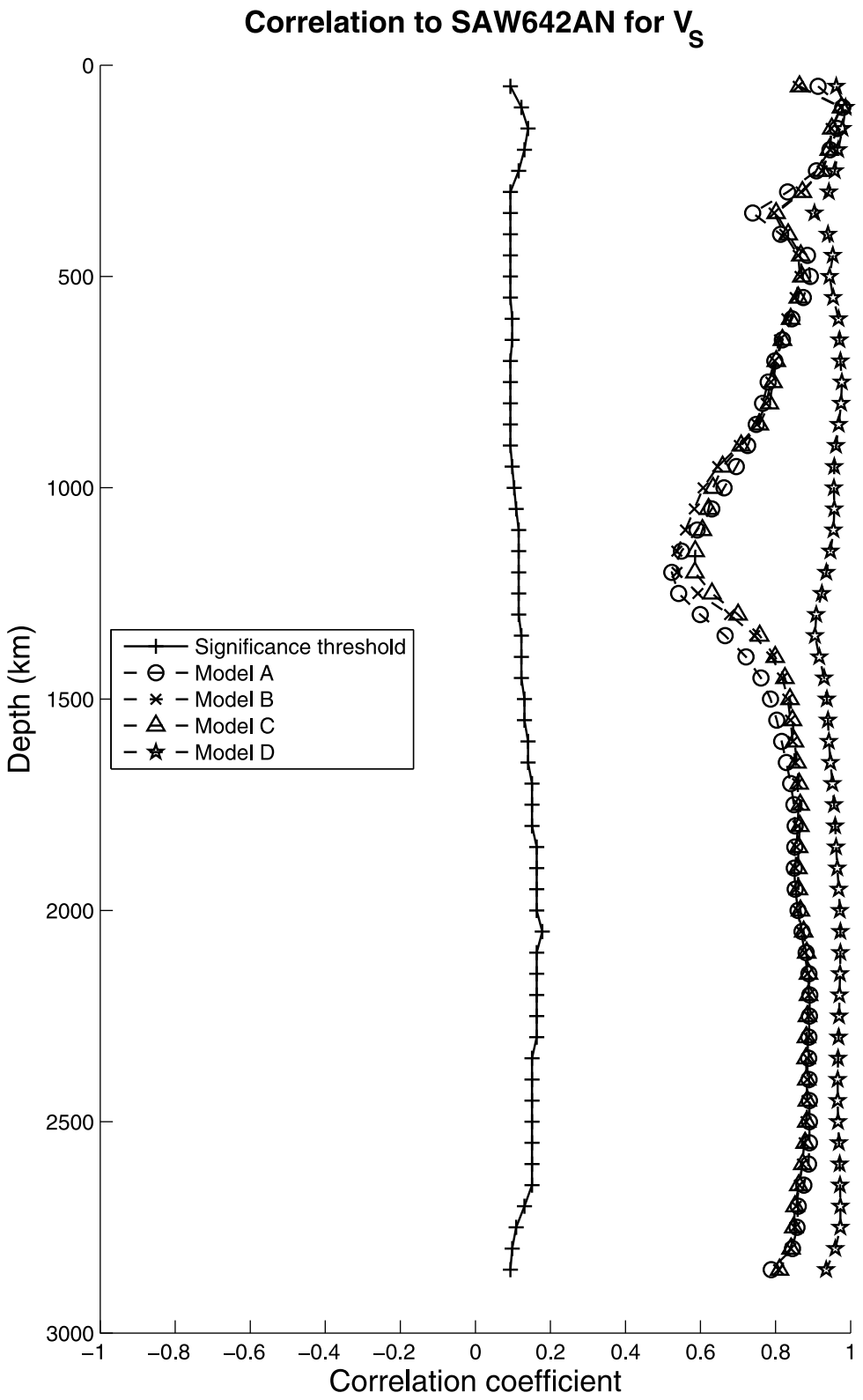

Figure 4. Correlation coefficient of the V_S models A, B, C, and D (dashed lines with symbols as defined in the legend) to SAW642AN as a function of depth up to spherical harmonic degree 24. The solid black line with pluses shows the 95% confidence threshold for significant correlation, calculated as described in the text.

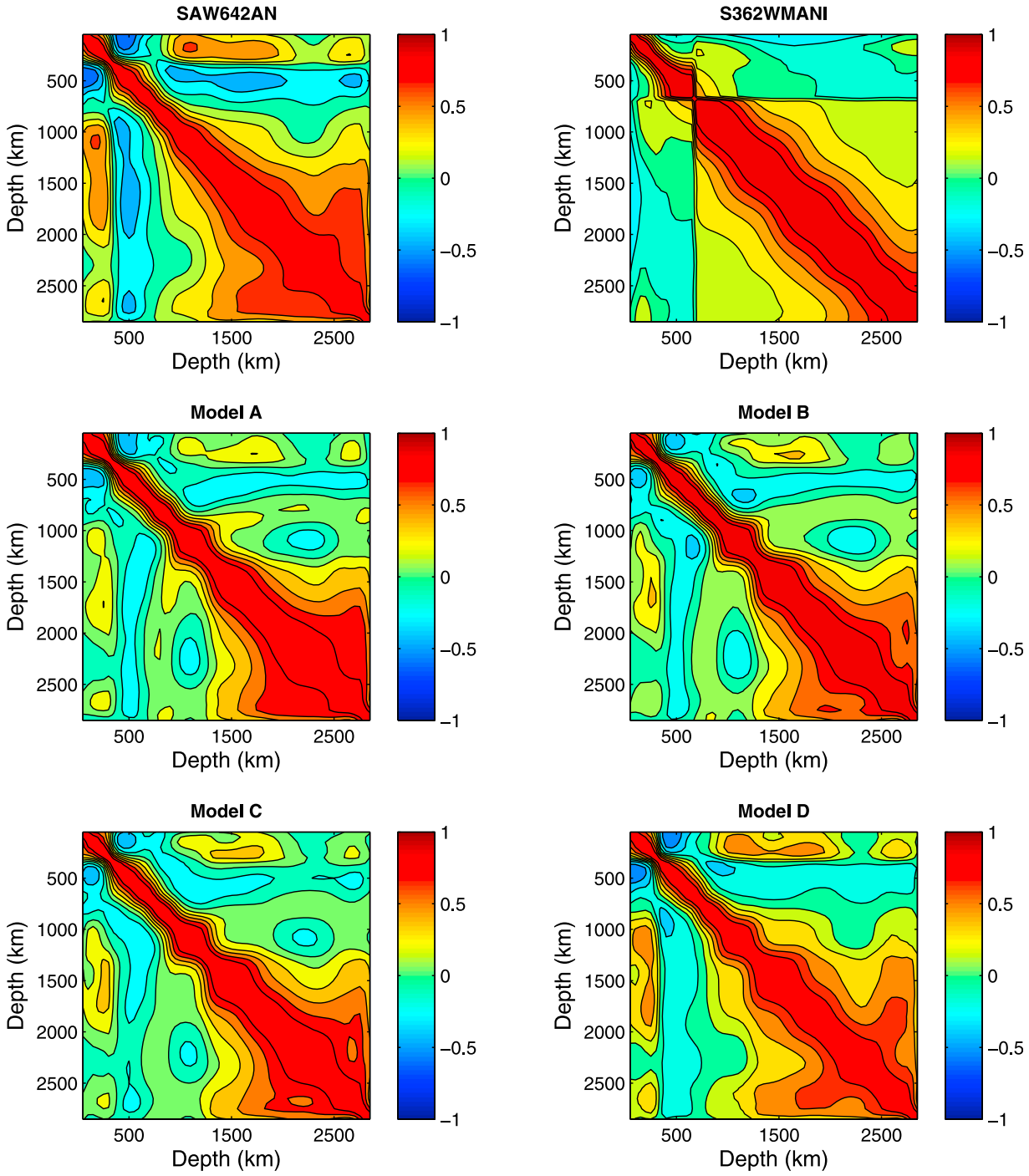

Figure 5. Radial correlation functions for isotropic V_S for SAW642AN, S362WMANI [*Kustowski et al.*, 2008] and models A, B, C, and D. Radial correlation functions graphically display the correlation between the structure in a model at different depths as represented by the values on the x and y axes.

S362WMANI [*Kustowski et al.*, 2008] (Figure 5). This signature is strongly reduced in models A–C, as shown in Figure 5, strongly suggesting that the MLC approach has reduced the effect of crustal artifacts. Model D, on the other hand, retains this signature (although with some reduction of the corresponding anticorrelation between transition zone structure and the deeper structure), suggesting that the crustal corrections for the body waves are the important controlling factor for this feature. Of course, there is still evidence for much more structure in the radial correlation functions for all models discussed here than for S362WMANI, but this is primarily due to the larger degree of smoothing present in that model.

3.2. Anisotropic Structure

[21] While the isotropic portion of the structure remained relatively robust regardless of crustal correction used, with the exception of the apparent removal of some artifacts in the

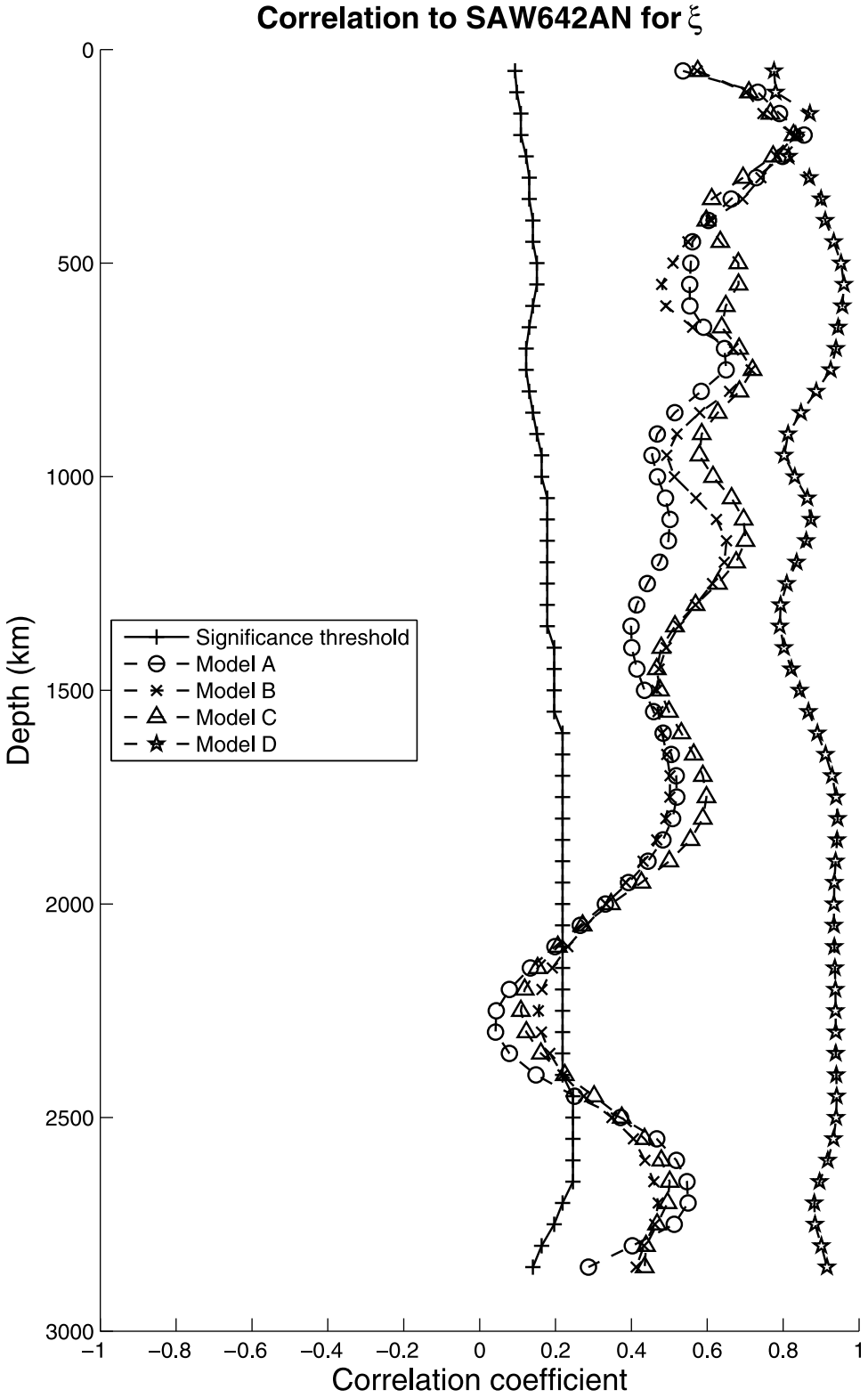

Figure 6. Same as Figure 4 but for the ξ parameter.

transition zone and upper part of the lower mantle, the changes are more pronounced in the anisotropic portion of the model (Figure 6).

[22] In the upper mantle, the correlations remain relatively high, generally ranging between 0.7 and 0.8 for models A, B, and C, and slightly higher for model D. In general, the signals in SAW642AN discussed by *Panning and Romanowicz* [2006] remain (Figure 7). We still image the positive ξ perturbation (i.e., V_{SH} increased relative to V_{SV}) beneath oceans at shallow depths that slowly decreases down to 300 km

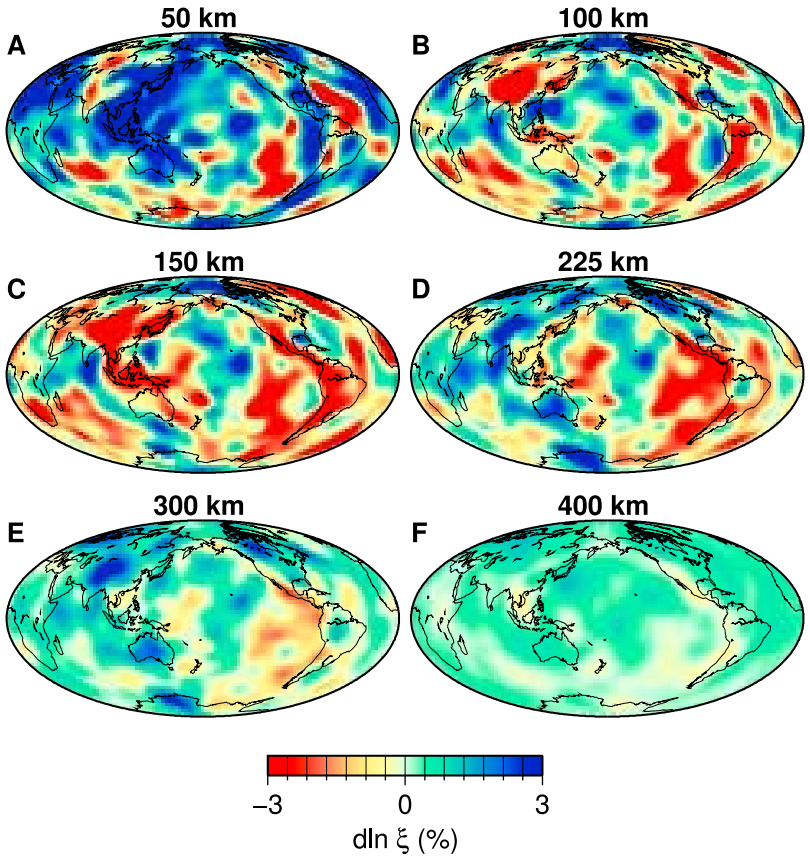

Figure 7. Perturbations in ξ relative to PREM (in percent) plotted for model B for several depths in the upper mantle.

depth, as well as the positive ξ perturbation beneath cratonic regions which is prominent between 200 and 300 km. These signatures remain consistent with the interpretation of focused deformation in the asthenosphere [*Gung et al.*, 2003]. We also still image the positive ξ perturbations beneath spreading centers between 150 and 200 km depth, which may be interpreted as a signal of vertical ridge feeding flow. These signatures appear to be robust to the different crustal corrections, and therefore we can continue to use them to make meaningful geodynamic inferences.

[23] The correlations are much lower in the transition zone and lower mantle. Model A, in particular, is less significantly correlated to SAW642AN throughout most of the lower mantle. Models B and C also have relatively low values of correlation throughout most of the lower mantle, generally ranging between 0.4 and 0.65, but all models are correlated with SAW642AN above the 95% confidence threshold except for a small range between 2000 and 2500 km depth, although we should once again note the caveat about the correlation significance thresholds, as discussed in section 3.1. Once again, model D, which has the same crustal corrections for body waves as SAW642AN, has very similar structure to SAW642AN throughout the transition zone and lower mantle.

[24] It is also interesting to look at the upper mantle radial correlation functions for ξ in the new models and compare them with SAW642AN and S362WMANI (Figure 8). *Bozdağ and Trampert* [2008] point out in their inversions that the spurious anisotropic structure due to inadequate crustal correction has a pronounced sign change between 50 and 150 km depth. The radial correlation functions show evidence of a sign change near 200 km depth (indicated by a small anticorrelation between structure above and below that depth) in SAW642AN and model A, as well as a possible sign change near 150 km depth in S362WMANI. Model D appears to show such a sign change a little deeper, near 300 km depth. No such sign change is apparent in models B or C. While there is no strong evidence to indicate that such a sign change does not reflect real Earth structure, it is another suggestion that model B shows less evidence of crustal artifacts than previous models. Ideally, we could attempt to quantitatively evaluate trade-offs between shallow structure and deeper structure in the different models to determine more accurately whether the observed anticorrelations are truly artifacts. One possible approach to this is to evaluate trade-offs using the resolution matrix, and see if such trade-offs are, for example, more pronounced for model A or D than for B or C. We attempted this (see auxiliary material), but the results simply demonstrated that there was little difference in the resolution matrices of the models.[1] Of course trade-off analysis using the resolution matrices for the different inversions only shows the differences due to problem geometry (which is identical for all cases), damping (which

[1] Auxiliary materials are available in the HTML. doi:10.1029/2010JB007520.

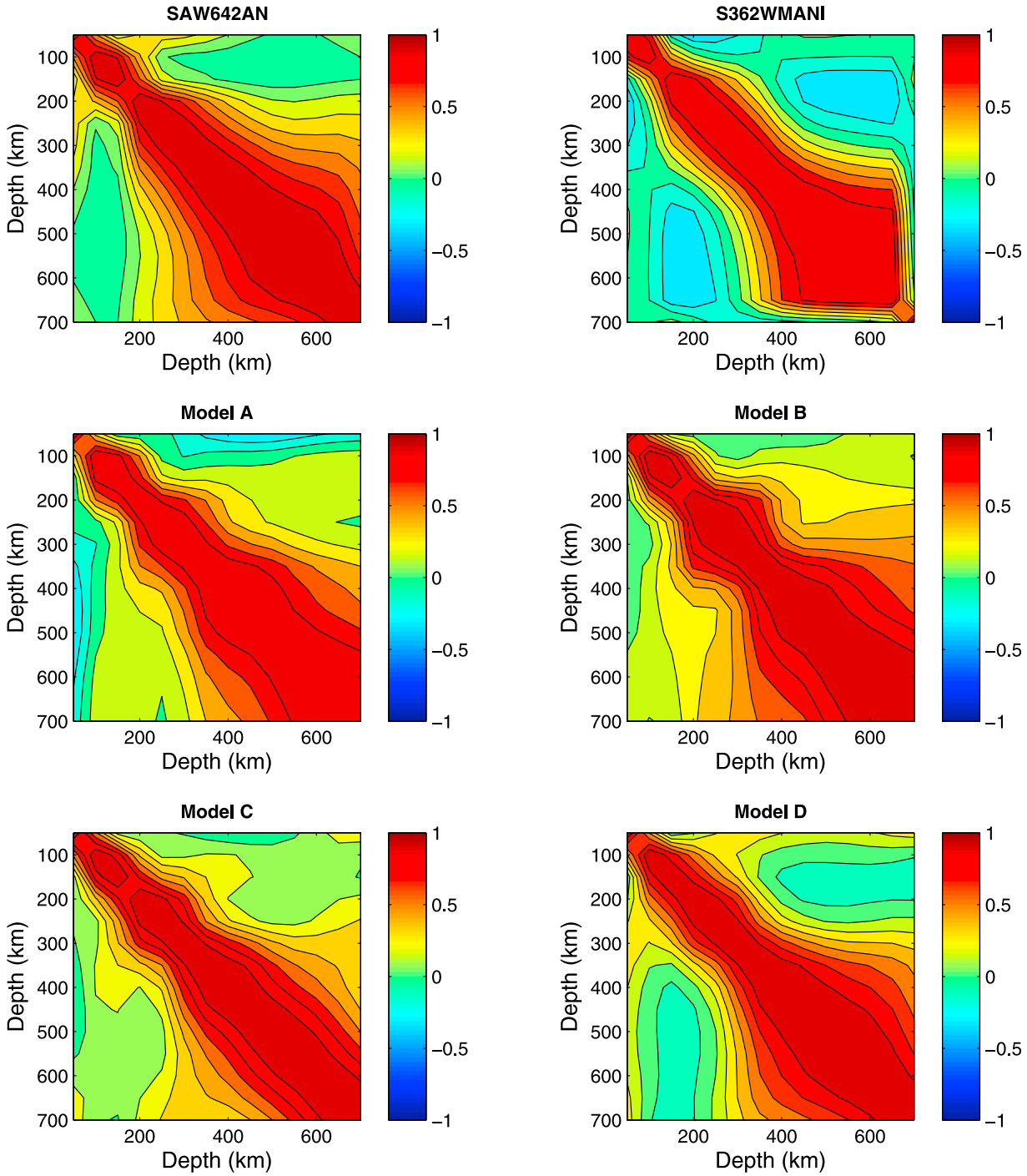

Figure 8. Upper mantle and transition zone radial correlation functions for ξ for SAW642AN, S362WMANI, and models A, B, C, and D.

does differ, although not by large margins) and theory used to calculate sensitivity (which is the same for models A–C but differs for SAW642AN and model D due to the use of kernels calculated in the regionalized models rather than PREM). It does not, however, directly address trade-offs that may appear due to real data not being adequately modeled by the particular choice of theory, such as the different approach to crustal corrections used here. These different theoretical approaches clearly cause significant changes to the resulting models although the resulting resolution matrices are all quite similar. Ideally, one could better address this issue by performing a test where the data set is recalculated using fully numerical synthetics and a known crustal model, however this is in many ways similar to the work done by *Bozdağ and Trampert* [2008] and *Lekić et al.* [2010], and beyond the scope of this study. Therefore, we cannot definitively conclude that the anticorrelation is indeed an artifact, but given the results of *Bozdağ and Trampert* [2008], it is cause for concern.

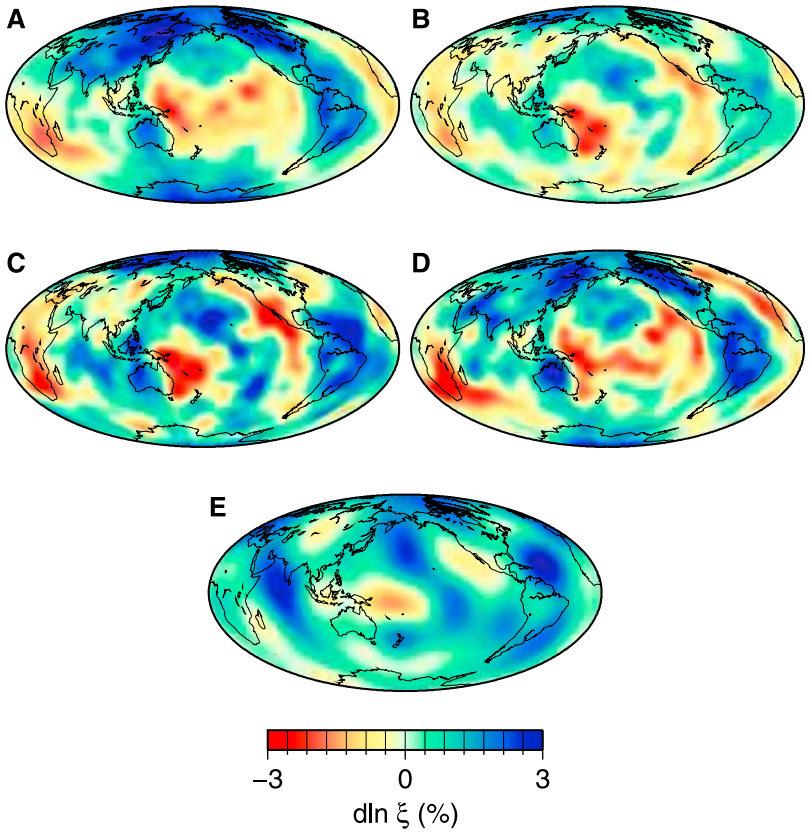

Figure 9. Perturbations in ξ at 2800 km depth plotted for (a) the SAW642AN, (b–d) models B, C, and D, and (e) cPR04. All perturbations are in percent relative to PREM.

[25] Because model B fits the data better than model A (with the caveats about statistical significance discussed in section 3), and reduces possible crustal artifacts, it appears that the use of overtone-based corrections to the body wave data produces a better model than using only linear corrections for the body wave portion of the data set, or using the NLC corrections used in the development of SAW642AN. While model B is our preferred model, all four models A through D will be made available through the first author's Web site.

[26] Because of the general decrease in correlation of anisotropic structure beginning at transition zone depths, we make the choice in models A and B to greatly increase the damping on ξ in this depth range, leading to the much lower amplitude of anisotropic structure compared with SAW642AN (Figure 2). Interestingly, we are still able to achieve better fit relative to SAW642AN to all data types with models A and B despite the smaller overall model size, which suggests the MLC corrections perform well relative to the NLC approach of MR07. Additionally, it calls into question whether significant anisotropy is required by the data through the transition zone and lower mantle, as already discussed based on attempts to resolve anisotropy using model space search techniques [*Beghein and Trampert*, 2004b]. However, we also inverted for model C, which was constrained to have a similar RMS amplitude of ξ structure to SAW642AN. As can be seen in Table 1, there is moderate improvement in fit using model C, but the correlation with SAW642AN remains relatively poor at transition zone and lower depths, making interpretation of such structure questionable. Model D has similar model size as model C, but with the same crustal corrections as SAW642AN for the body waves, and therefore much stronger correlation throughout the transition zone and lower mantle. Overall, there is some improvement in fit for model D relative to SAW642AN, although not as much as for models A–C. In detail, most of the improvement in fit in model D relative to SAW642AN is in the surface waves, while the body waves show only marginal improvement. When this is combined with previous tests showing that anisotropic structure in the lower transition zone and uppermost lower mantle is also sensitive to trade-offs related to the use of scaling parameters and choices in model parameterization [*Panning and Romanowicz*, 2006; *Beghein*, 2010], we choose to adopt the more conservative model B as our preferred model, which we call SAW642ANb.

3.3. Core-Mantle Boundary Region

[27] While amplitudes of ξ structure were constrained to be low throughout the bulk of the lower mantle, previous work has suggested that including some anisotropic structure in the core-mantle boundary region (D″) led to significant improvement in fit for the portion of the body wave data set sensitive to D″ structure relative to a model constrained to be isotropic throughout the lower mantle [*Panning and Romanowicz*, 2004, 2006]. For this reason, all three models still allow for ξ structure in the lowermost mantle (shown in Figure 9 for model B). Once again, there are very broad

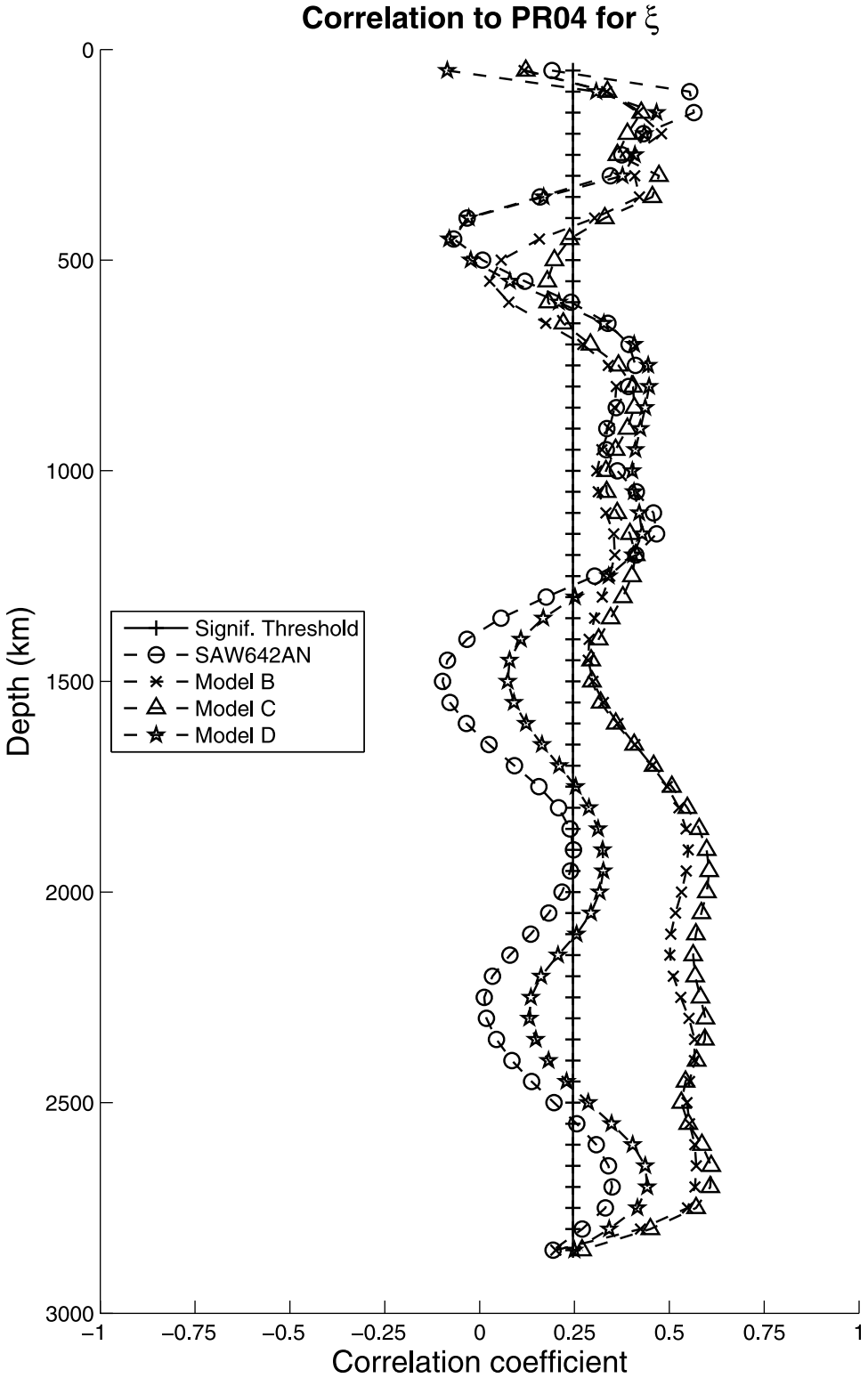

Figure 10. Same as Figure 6 but plotting correlations relative to model PR04 for SAW642AN and models B, C, and D (dashed lines with symbols as defined in the legend).

similarities with the structure resolved in SAW642AN, but there are significant differences, as emphasized by the relatively low correlation values ranging between 0.4 and 0.5 for models B and C relative to SAW642AN (Figure 6). Interestingly, some of the largest apparent visual differences, such as the band of positive ξ running through the central Pacific, and the negative ξ under much of Asia appear more similar to the model PR04 developed with only linear corrections (Figure 9a).

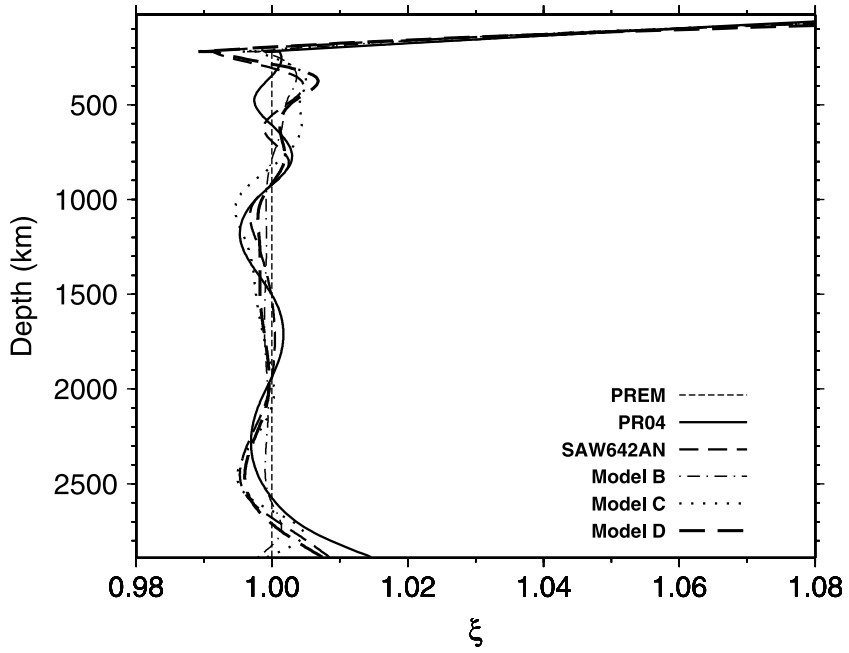

Figure 11. Spherically symmetric ξ signature through the mantle for PREM (thin black dashed line) as well as models PR04 (solid black line), SAW642AN (medium dashed line), model B (dash-dotted line), model C (dotted line), and model D (thick dashed line).

[28] In order to explore this further, we calculated correlations of SAW642AN and models B and C to PR04 up to the maximum resolution of that model, spherical harmonic degree 8 (Figure 10). While SAW642AN is generally decorrelated from PR04 throughout the lower mantle, models B and C show much greater correlation, ranging from 0.6 to 0.7 with the exception of the structure resolved in the lowermost spline in both models.

[29] Another concern in this depth range is resolution. The structure in this depth range is primarily controlled by SKS and core diffracted S phases, as well as some multiple ScS phases. While coverage is in general better in the lowermost mantle than in much of the midmantle [*Panning and Romanowicz*, 2006, Figure 2], checkerboard resolution tests suggest that there may be some contamination due to isotropic velocity structure (see auxiliary material).

[30] Such concerns and the differences between the models of D″ anisotropy developed with three different crustal correction choices could also bring into question the signal of spherically averaged positive ξ in this depth range, which we previously considered to be a robust conclusion [*Panning and Romanowicz*, 2004, 2006]. While contamination from isotropic velocity seems to be unlikely, as there is no comparable strong mean signal in the V_S profile, we can see that the average signature is almost absent in model B (Figure 11), and is shifted to shallower depths in model C. This is, of course, a consequence of the choice to more heavily damp anisotropic structure at transition zone and greater depths in model B relative to SAW642AN or model C. Additionally, as pointed out before, the applicability of the MLC approach to body waves is inherently problematic, and so previous models of lower mantle anisotropic structure may actually be preferred. Model D uses the previous NLC corrections for the body waves, and results in D″ much more similar to SAW642AN, both in terms of 3-D structure and 1-D average. Finally, there are multiple independent lines of evidence for widespread presence of $V_{SH} > V_{SV}$ in D″ based on detailed analysis of waveforms sampling the region [e.g., *Lay et al.*, 1998]. In general, however, it appears that the specific details of D″ anisotropy in a global tomographic model are quite sensitive to the choice of crustal corrections, and therefore potentially problematic to interpret.

4. Discussion

[31] The sensitivity of resolved mantle anisotropic structure to the method of crustal correction used implies that crustal corrections may currently be a limiting factor for improved resolution and agreement between models of mantle anisotropy. Isotropic structure appears to be relatively robust as indicated by its greater stability in this study as well as the broad convergence of models from different research groups using different data sets and different approaches to crustal structure. However, it is apparent that moving to finer resolution or including second-order structure such as anisotropy or attenuation will require very accurate crustal corrections. The difficulties presented by crustal structure for radially anisotropic models as in this study also likely indicate that crustal corrections will be even more important for robust determination of models using more ambitious anisotropic parameterizations including arbitrarily oriented symmetry axes [*Montagner and Nataf*, 1988; *Sieminski et al.*, 2007; *Panning and Nolet*, 2008].

[32] Of course, one avenue of improving crustal corrections has to be improving our knowledge of the real structure of the Earth's crust. A recent study by *Ferreira et al.* [2010] showed differences between radially anisotropic models developed using different models for the crust, particularly in the top 100 km of the mantle. In this case, the methodology of using

local eigenfunction calculations along a great circle path [e.g., *Boschi and Ekström*, 2002] was used to correct a large data set of fundamental and overtone surface wave phase velocity measurements for three different published global crustal models. The resulting models had some noticeable differences, particularly in the 100 km depth range, while differences in crustal models had as much impact on fit to the data as including radial anisotropy. For long-period waveform data sets such as the one used in this modeling, improving crustal models may partially be accomplished by moving from models derived from more localized studies and tectonic inference, such as CRUST5.1 [*Mooney et al.*, 1998] and CRUST2.0 [*Bassin et al.*, 2000] to models derived specifically from global surface wave data sets [e.g., *Meier et al.*, 2007], although *Ferreira et al.* [2010] suggests that model may actually result in a poorer fit. However, SAW642AN and the models discussed in this study are derived from different implementations of nonlinear crustal corrections, but starting from the same crustal model, CRUST2.0. The differences between the models implies that we need to not only seek to improve the crustal models used for correction, but importantly to focus on which methods of applying crustal corrections are up to the task.

[33] Allowing for inversion for further Moho perturbations is another specific methodological tool used in previous models developed using NACT to improve crustal corrections [*Li and Romanowicz*, 1996; *Mégnin and Romanowicz*, 2000]. These Moho perturbations were not intended to be interpreted, but rather to act as a 'trash can' in which to dump unmodeled crustal structure. This particular approach is not well-suited for use with the MLC approach, however. The MLC method explicitly uses multiple sets of Moho perturbations for different mode types, and thus an inversion for a new single set of Moho perturbations is poorly formed, and would throw out the nonlinear crustal corrections for any further iteration. However, such an approach was tested as well (see auxiliary material) but did not lead to significant changes in the output models or fit to the data.

[34] The improved data fit and removal of apparent crustal artifacts relative to SAW642AN are strong evidence that the MLC correction approach performs better for this data set than the NLC corrections used in the earlier model. Interestingly, this improved fit and removal of apparent crustal artifacts seems to require the MLC corrections be applied to both the surface waves and body waves in the data set, as model D, which used the NLC corrections for the body waves has similar data fit and radial correlation functions to SAW642AN. It is not clear, however, exactly how to explain this difference. Both methods attempt to account for the nonlinear effects of crustal structure modeled as boundary perturbations of the Moho and surface topography. Only the NLC approach, however, directly includes the effect of different crustal structure on the sensitivity kernels to deep structure, which would seem to offer improvement relative to the approach used here. However, the higher computational costs of the NLC approach did lead to the use of a smaller set of regionalized models (5 versus 7 in this study), and it is possible some of the differences may result from that. It is also possible that the improvement results from some sort of fortuitous cancelation of errors, where any errors introduced by the MLC approach are somehow complementary to errors introduced through any inadequacies of CRUST2.0. Finally, it is also possible that there was some error in the implementation of NLC in the development of SAW642AN. Further study is warranted in order to understand this, but the way forward has to include better ways of fully incorporating the nonlinear effect of crustal structure on the waveforms. One possibility for this is to utilize numerical tools such as the spectral element method [e.g., *Komatitsch and Vilotte*, 1998] in the forward calculations which would incorporate all nonlinear effects on the wavefield provided we have accurate enough crustal models, while still using analytical approaches for the partial derivatives used in the inversion (V. Lekić and B. Romanowicz, Inferring upper mantle structure by full waveform tomography with the spectral element method, submitted to *Geophysical Journal International*, 2010). Another avenue which will require taking advantage of ever-increasing computational power is to utilize a fully numerical inverse approach such as the adjoint inversion proposed by *Tromp et al.* [2005]. While many recent studies have focused on improvements to tomography based upon the use of 3-D finite frequency sensitivity kernels [*Montelli et al.*, 2006; *Zhou et al.*, 2006], using such approaches for crustal structure will likely not offer significant improvement, as these remain strictly a linear approach [e.g., *Panning et al.*, 2009], and as such are likely inadequate to correct for the effects of crustal structure.

[35] While there is strong evidence that the preferred model in this study, SAW642ANb, is an improvement relative to SAW642AN, we need to consider very carefully whether the anisotropic structure at all depth ranges can be considered reliable. Clearly the overall fit to the data has improved, and the isotropic model in particular appears to show less indication of crustal contamination. Routine tests of model quality, such as resolution matrix checkerboard tests and bootstrap error maps (see auxiliary material), indicate results very similar to SAW642AN for the isotropic structure, although the apparent resolution of lower mantle anisotropic structure is naturally reduced because we choose to increase damping for this depth range. Additionally, lower mantle structure obviously depends most strongly on the body wave data set, and despite the improved fits, there are still theoretical reasons to question the application of the MLC approach to body waves due to the implicit assumption of self-coupling of modes. Attempting to use MLC for the surface waves and NLC for the body waves (model D), however, does not show the apparent reduction in artifacts shown in models B and C. Perhaps the difference is partially related to the larger number of regionalized models possible in the MLC approach, but this is not certain. Taken together, these concerns indicate that there remains a lot of room for improvement in global anisotropic models, particularly at large depths, and that interpretation of anisotropic structure below upper mantle depths should not be taken lightly.

5. Conclusions

[36] We have applied a new method of crustal corrections to the same three-component waveform data set used in the creation of SAW642AN. By comparing models derived using different crustal corrections, we have shown that crustal corrections have the potential for substantially affecting the retrieved anisotropic structure even in the lower mantle. Our

preferred model, SAW642ANb, shows improved data fit and evidence of fewer crustal artifacts. Because of the sensitivity of resolved anisotropic structure at transition zone and greater depths to the choice of crustal corrections, we prefer a model with anisotropic structure more strongly damped than in previous modeling. Despite the overall smaller model size of this new model (as determined from RMS amplitude of structure as a function of depth), the fit to all data types is improved relative to SAW642AN.

[37] **Acknowledgments.** This research was partially supported by NSF grant EAR-0911414. Support for V.L. provided in part by NSF Graduate Fellowship.

References

Bassin, C., G. Laske, and G. Masters (2000), The current limits of resolution for surface wave tomography in North America, *Eos Trans. AGU*, *81*(48), Fall Meet. Suppl., Abstract S12A-03.

Becker, T., B. Kustowski, and G. Ekström (2008), Radial seismic anisotropy as a constraint for upper mantle rheology, *Earth Planet. Sci. Lett.*, *267*, 213–227, doi:10.1016/j.epsl.2007.11.038.

Beghein, C. (2010), Radial anisotropy and prior petrological constraints: A comparative study, *J. Geophys. Res.*, *115*, B03303, doi:10.1029/2008JB005842.

Beghein, C., and J. Trampert (2004a), Probability density functions for radial anisotropy for fundamental mode surface wave data and the Neighbourhood Algorithm, *Geophys. J. Int.*, *157*, 1163–1174, doi:10.1111/j.1365-246X.2004.02235.x.

Beghein, C., and J. Trampert (2004b), Probability density functions for radial anisotropy: Implications for the upper 1200 km of the Earth, *Earth Planet. Sci. Lett.*, *217*, 151–162, doi:10.1016/S0012-821X(03)00575-2.

Beghein, C., J. Resovsky, and R. van der Hilst (2008), The signal of mantle anisotropy in the coupling of normal modes, *Geophys. J. Int.*, *175*, 1209–1234, doi:10.1111/j.1365-246X.2008.03970.x.

Boschi, L., and A. Dziewonski (2000), Whole Earth tomography from delay times of P, PcP, and PKP phases: Lateral heterogeneities in the outer core or radial anisotropy in the mantle?, *J. Geophys. Res.*, *105*(B6), 13,675–13,696, doi:10.1029/2000JB900059.

Boschi, L., and G. Ekström (2002), New images of the Earth's upper mantle from measurements of surface wave phase velocity anomalies, *J. Geophys. Res.*, *107*(B4), 2059, doi:10.1029/2000JB000059.

Bozdağ, E., and J. Trampert (2008), On crustal corrections in surface wave tomography, *Geophys. J. Int.*, *172*, 1066–1082, doi:10.1111/j.1365-246X.2007.03690.x.

Ferreira, A. M. G., J. H. Woodhouse, K. Visser, and J. Trampert (2010), On the robustness of global radially anisotropic surface wave tomography, *J. Geophys. Res.*, *115*, B04313, doi:10.1029/2009JB006716.

Gu, Y., A. Dziewonski, and G. Ekström (2003), Simultaneous inversion for mantle shear velocity and topography of transition zone discontinuities, *Geophys. J. Int.*, *154*, 559–583, doi:10.1046/j.1365-246X.2003.01967.x.

Gung, Y., M. Panning, and B. Romanowicz (2003), Global anisotropy and the thickness of continents, *Nature*, *422*, 707–711, doi:10.1038/nature01559.

Houser, C., G. Masters, P. Shearer, and G. Laske (2008), Shear and compressional velocity models of the mantle from cluster analysis of long-period waveforms, *Geophys. J. Int.*, *174*, 195–212, doi:10.1111/j.1365-246X.2008.03763.x.

Kaminski, E., and N. Ribe (2001), A kinematic model for recrystallization and texture development in olivine polycrystals, *Earth Planet. Sci. Lett.*, *189*, 253–267, doi:10.1016/S0012-821X(01)00356-9.

Karato, S.-I., H. Jung, I. Katayama, and P. Skemer (2008), Geodynamic significance of seismic anisotropy of the upper mantle: New insights from laboratory studies, *Annu. Rev. Earth Planet. Sci.*, *36*, 59–95, doi:10.1146/annurev.earth.36.031207.124120.

Komatitsch, D., and J.-P. Vilotte (1998), The spectral-element method: an efficient tool to simulate the seismic response of 2D and 3D geological structures, *Bull. Seismol. Soc. Am.*, *88*(2), 368–392.

Kustowski, B., A. Dziewoński, and G. Ekström (2007), Nonlinear crustal corrections for normal-mode seismograms, *Bull. Seismol. Soc. Am.*, *97*(5), 1756–1762, doi:10.1785/0120070041.

Kustowski, B., G. Ekström, and A. M. Dziewoński (2008), Anisotropic shear wave velocity structure of the Earth's mantle: A global model, *J. Geophys. Res.*, *113*, B06306, doi:10.1029/2007JB005169.

Lay, T., Q. Williams, E. Garnero, L. Kellogg, and M. Wysession (1998), Seismic wave anisotropy in the D″ region and its implications, in *The Core-Mantle Boundary Region*, *Geodyn. Ser.*, vol. 28, edited by M. Gurnis et al., pp. 299–318, AGU, Washington, D. C.

Lekić, V., M. Panning, and B. Romanowicz (2010), A simple method for improving crustal corrections in waveform tomography, *Geophys. J. Int.*, *182*, 265–278, doi:10.1111/j.1365-246X.2010.04602.x.

Li, C., R. van der Hilst, and M. Toksöz (2006), Constraining P-wave velocity variation in the upper mantle beneath Southeast Asia, *Phys. Earth Planet. Inter.*, *154*, 180–195, doi:10.1016/j.pepi.2005.09.008.

Li, X.-D., and B. Romanowicz (1995), Comparison of global waveform inversions with and without considering cross-branch modal coupling, *Geophys. J. Int.*, *121*, 695–709, doi:10.1111/j.1365-246X.1995.tb06432.x.

Li, X.-D., and B. Romanowicz (1996), Global mantle shear velocity model developed using nonlinear asymptotic coupling theory, *J. Geophys. Res.*, *101*(B10), 22,245–22,272, doi:10.1029/96JB01306.

Marone, F., and B. Romanowicz (2007), Non-linear crustal correction in high-resolution regional waveform seismic tomography, *Geophys. J. Int.*, *170*(1), 460–467, doi:10.1111/j.1365-246X.2007.03399.x.

Mégnin, C., and B. Romanowicz (1999), The effect of theoretical formalism and data selection scheme on mantle models derived from waveform tomography, *Geophys. J. Int.*, *138*, 366–380, doi:10.1046/j.1365-246X.1999.00869.x.

Mégnin, C., and B. Romanowicz (2000), The 3D shear velocity structure of the mantle from the inversion of body, surface, and higher mode waveforms, *Geophys. J. Int.*, *143*, 709–728, doi:10.1046/j.1365-246X.2000.00298.x.

Meier, U., A. Curtis, and J. Trampert (2007), Fully nonlinear inversion of fundamental mode surface waves for a global crustal model, *Geophys. Res. Lett.*, *34*, L16304, doi:10.1029/2007GL030989.

Montagner, J.-P., and N. Jobert (1988), Vectorial tomography: II. Application to the Indian Ocean, *Geophys. J. R. Astron. Soc.*, *94*, 309–344.

Montagner, J.-P., and H.-C. Nataf (1988), Vectorial tomography: I. Theory, *Geophys. J. R. Astron. Soc.*, *94*, 295–307.

Montelli, R., G. Nolet, F. Dahlen, G. Masters, E. Engdahl, and S.-H. Hung (2004), Finite-frequency tomography reveals a variety of plumes in the mantle, *Science*, *303*, 338–343, doi:10.1126/science.1092485.

Montelli, R., G. Nolet, F. Dahlen, and G. Masters (2006), A catalogue of deep mantle plumes: New results from finite-frequency tomography, *Geochem. Geophys. Geosyst.*, *7*, Q11007, doi:10.1029/2006GC001248.

Mooney, W., G. Laske, and G. Masters (1998), CRUST 5.1: A global crustal model at 5 × 5 degrees, *J. Geophys. Res.*, *103*, 727–747, doi:10.1029/97JB02122.

Panning, M., and G. Nolet (2008), Surface wave tomography for azimuthal anisotropy in a strongly reduced parameter space, *Geophys. J. Int.*, *174*(2), 629–648, doi:10.1111/j.1365-246X.2008.03833.x.

Panning, M., and B. Romanowicz (2004), Inferences on flow at the base of Earth's mantle based on seismic anisotropy, *Science*, *303*, 351–353, doi:10.1126/science.1091524.

Panning, M., and B. Romanowicz (2006), A three-dimensional radially anisotropic model of shear velocity in the whole mantle, *Geophys. J. Int.*, *167*, 361–379, doi:10.1111/j.1365-246X.2006.03100.x.

Panning, M., Y. Capdeville, and B. Romanowicz (2009), Seismic waveform modelling in a 3-D Earth using the Born approximation: Potential shortcomings and a remedy, *Geophys. J. Int.*, *177*, 161–178, doi:10.1111/j.1365-246X.2008.04050.x.

Park, J. (1993), The sensitivity of seismic free oscillations to upper mantle anisotropy: 1. Zonal symmetry, *J. Geophys. Res.*, *98*(B11), 19,933–19,949, doi:10.1029/93JB02177.

Ritsema, J., H. J. van Heijst, and J. H. Woodhouse (2004), Global transition zone tomography, *J. Geophys. Res.*, *109*, B02302, doi:10.1029/2003JB002610.

Romanowicz, B., M. Panning, Y. Gung, and Y. Capdeville (2008), On the computation of long period seismograms in a 3D Earth using normal mode based approximations, *Geophys. J. Int.*, *175*(2), 520–536, doi:10.1111/j.1365-246X.2008.03914.x.

Sieminski, A., Q. Liu, J. Trampert, and J. Tromp (2007), Finite-frequency sensitivity of surface waves to anisotropy based upon adjoint methods, *Geophys. J. Int.*, *168*, 1153–1174, doi:10.1111/j.1365-246X.2006.03261.x.

Simmons, N., A. Forte, and S. Grand (2009), Joint seismic, geodynamic and mineral physical constraints on three-dimensional mantle heterogeneity: Implications for the relative importance of thermal versus compositional heterogeneity, *Geophys. J. Int.*, *177*, 1284–1304, doi:10.1111/j.1365-246X.2009.04133.x.

Tromp, J., C. Tape, and Q. Liu (2005), Seismic tomography, adjoint methods, time reversal and banana-doughnut kernels, *Geophys. J. Int.*, *160*, 195–216, doi:10.1111/j.1365-246X.2004.02453.x.

Wang, Z., and F. Dahlen (1995), Spherical-spline parameterization of three-dimensional Earth models, *Geophys. Res. Lett.*, *22*(22), 3099–3102, doi:10.1029/95GL03080.

Zhou, Y., G. Nolet, F. Dahlen, and G. Laske (2006), Global upper-mantle structure from finite-frequency surface-wave tomography, *J. Geophys. Res.*, *111*, B04304, doi:10.1029/2005JB003677.

V. Lekić, Department of Geological Sciences, Brown University, 324 Brook St., Providence, RI 02912, USA.

M. P. Panning, Department of Geological Sciences, University of Florida, 241 Williamson Hall, PO Box 112120, Gainesville, FL 32611, USA. (mpanning@ufl.edu)

B. A. Romanowicz, Berkeley Seismological Laboratory, University of California, McCone Hall 215, Berkeley, CA 94720, USA.